Free-carrier absorption in transparent conducting oxides: Phonon and impurity scattering in SnO_{2}

H. Peelaers, E. Kioupakis, and C. G. Van de Walle

Phys. Rev. B **92**, 235201 — Published 2 December 2015

DOI: 10.1103/PhysRevB.92.235201

Free-carrier absorption in transparent conducting oxides: phonon and impurity scattering in SnO_2

H. Peelaers,[1,*] E. Kioupakis,[1,2] and C. G. Van de Walle[1]

[1] *Materials Department, University of California, Santa Barbara, CA 93106-5050*
[2] *Department of Materials Science and Engineering, University of Michigan, Ann Arbor, Michigan 48109, USA*

(Dated: November 16, 2015)

Indirect absorption plays an important role in the transparency of transparent conducting oxides. We provide a detailed first-principles study of phonon- and charged-impurity-assisted free-carrier absorption, with the example of SnO_2. The dominant phonon modes contributing to the electron-phonon coupling are identified and are used to assess the validity of the Fröhlich model. We find that phonon-assisted indirect absorption dominates if the ionized dopant concentration is below 10^{20} cm^{-3}, and that phonon emission dominates this process. We also discuss subtle but important issues relating to the calculation of optical transition matrix elements.

PACS numbers: 78.40.Fy,78.20.Bh,63.20.kd,63.20.dk

I. INTRODUCTION

Optoelectronic devices invariably require metallic contacts to apply voltage and conduct current into and out of the device. By nature, metals are opaque; any area where metallic contacts are applied is therefore no longer transparent to light, thus limiting the efficiency of either light emission or light absorption. Transparent contacts would solve this problem, and they can indeed be achieved with materials that are essentially highly doped wide-band-gap semiconductors. Their large band gap renders them transparent to visible (or even ultraviolet) light, while the large carrier concentration (usually electrons) provides a high conductivity. The class of materials that exhibits this combination of contraindicated properties (high transparency and high conductivity) is relatively small, and consists mainly of oxides; hence the label "transparent conducting oxides" (TCOs). They are used in applications ranging from solar cells, displays, smart windows, and touch screens to light-emitting diodes.[1–4]

In TCOs such as In_2O_3, SnO_2, and ZnO, the energy at which absorption of photons can lead to excitation of electrons from the valence band into the conduction band) is above the visible region. What is often overlooked in the consideration of the transparency criterion is that the free carriers that need to be present to ensure high conductivity can also absorb photons. Checking whether direct transitions from the filled states at the conduction-band minimum to higher conduction bands are allowed is fairly straightforward. *Indirect* transitions can also lead to significant absorption, however—as is evident from the use of indirect-band-gap materials such as silicon in photovoltaics.[5] The large concentration of electrons in the conduction band, combined with the potentially large density of states available throughout the Brillouin zone that are made accessible in indirect processes, can lead to sizable absorption that sets a fundamental limit on the transparency of the TCO.

Figure 1(a) displays the band structure of SnO_2, which has a band gap of 3.6 eV.[6,7] Direct transitions from the bottom of the conduction band to the higher-lying conduction band would require a photon energy of more than 4.7 eV, and thus cannot lead to absorption of visible light. Indirect transitions, in which momentum is supplied by a scattering process, are possible to states throughout the zone, however. We will consider two important indirect processes here: those mediated by phonons and those due to scattering by ionized impurities. The latter are unavoidably present due to the doping necessary to obtain the high carrier concentration.

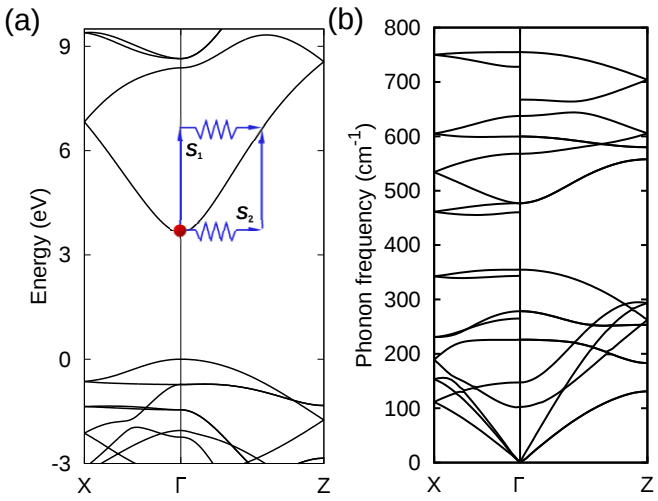

FIG. 1. (Color online) (a) Band structure of SnO_2 in the directions parallel to c (Γ-Z) and perpendicular to c (Γ-X). The two processes that lead to the generalized optical matrix elements $\boldsymbol{S}_1$ [Eq. (2)] and $\boldsymbol{S}_2$ [Eq. (3)] are indicated. (b) The phonon spectrum plotted along the same directions as in (a).

Indirect absorption is usually described by the Drude model. This phenomenological theory works well in the infrared, but is based on scattering parameters fitted to experiment and hence cannot be applied to novel materials that have not yet been experimentally explored. In

addition, it cannot be used in the visible or ultraviolet, where band-structure effects are important. Other models can be constructed for specific scattering processes,[8] but these also contain phenomenological parameters. A first-principles description is thus called for. We have developed such a methodology and have previously reported results for nitrides[9,10] and SnO_2.[11] Those results focused on phonon-assisted absorption. In the present paper we go beyond the previous work by i) addressing charged-impurity-assisted absorption and its comparison to the phonon-assisted absorption, ii) providing a more detailed discussion of the computational approach, iii) assessing the validity of the widely used Fröhlich model, iv) discussing the magnitude of the different possible absorption processes, such as emission *versus* absorption of a phonon, v) analyzing the temperature dependence, and vi) discussing computational pitfalls related to the optical transition matrix elements. The examples in this paper focus on SnO_2, but the formalism is general.

II. TECHNICAL DETAILS

A. Formalism

To calculate the phonon-assisted absorption coefficient from first principles, we use Fermi's golden rule:[9,12]

$$\alpha(\omega) = 2\frac{4\pi^2 e^2}{\omega c n_r(\omega)} \frac{1}{V_{\text{cell}}} \frac{1}{N_{\boldsymbol{k}} N_{\boldsymbol{q}}} \sum_{\nu i j \boldsymbol{k}\boldsymbol{q}} |\hat{\boldsymbol{e}} \cdot (\boldsymbol{S}_1 + \boldsymbol{S}_2)|^2 \times P\delta(\epsilon_{j,\boldsymbol{k}+\boldsymbol{q}} - \epsilon_{i\boldsymbol{k}} - \hbar\omega \pm \hbar\omega_{\nu\boldsymbol{q}}), \quad (1)$$

where $\hbar\omega$ and $\hat{\boldsymbol{e}}$ are the energy and polarization of the photon, $n_r(\omega)$ the refractive index of SnO_2 at frequency ω, $\hbar\omega_{\nu\boldsymbol{q}}$ the phonon energy, and $\epsilon_{i\boldsymbol{k}}$ the electron energy. Indices i and j indicate the band number, ν the phonon mode, and $\boldsymbol{k}$ and $\boldsymbol{q}$ the wave vectors. The generalized optical matrix elements, $\boldsymbol{S}_1$ and $\boldsymbol{S}_2$, are given by

$$\boldsymbol{S}_1(\boldsymbol{k},\boldsymbol{q}) = \sum_m \frac{\boldsymbol{v}_{im}(\boldsymbol{k}) g^{\text{el-ph}}_{mj,\nu}(\boldsymbol{k},\boldsymbol{q})}{\epsilon_{m\boldsymbol{k}} - \epsilon_{i\boldsymbol{k}} - \hbar\omega}, \quad (2)$$

$$\boldsymbol{S}_2(\boldsymbol{k},\boldsymbol{q}) = \sum_m \frac{g^{\text{el-ph}}_{im,\nu}(\boldsymbol{k},\boldsymbol{q}) \boldsymbol{v}_{mj}(\boldsymbol{k}+\boldsymbol{q})}{\epsilon_{m,\boldsymbol{k}+\boldsymbol{q}} - \epsilon_{i\boldsymbol{k}} \pm \hbar\omega_{\nu\boldsymbol{q}}}, \quad (3)$$

and correspond to the two possible paths of the indirect absorption process (Fig. 1). They are determined in terms of the optical ($\boldsymbol{v}$) and electron-phonon coupling ($g^{\text{el-ph}}$) matrix elements. The electron-phonon coupling matrix elements are given by

$$g^{\text{el-ph}}_{ij,\nu}(\boldsymbol{k},\boldsymbol{q}) = \sqrt{\frac{\hbar}{2M\omega_{\nu\boldsymbol{q}}}} \langle i,\boldsymbol{k}|\partial_{\nu,\boldsymbol{q}} V|j,\boldsymbol{k}+\boldsymbol{q}\rangle, \quad (4)$$

where M is the atomic mass and $\partial_{\nu,\boldsymbol{q}} V$ the phonon deformation potential. The factor P accounts for the carrier and phonon statistics,

$$P = \left(n_{\nu\boldsymbol{q}} + \frac{1}{2} \pm \frac{1}{2}\right)(f_{i\boldsymbol{k}} - f_{j,\boldsymbol{k}+\boldsymbol{q}}). \quad (5)$$

Here $n_{\nu\boldsymbol{q}}$ and $f_{i\boldsymbol{k}}$ are the phonon and electron occupation numbers. The upper (lower) sign corresponds to phonon emission (absorption).

We describe the ionized impurity scattering based on a model screened Coulomb potential.[13] The corresponding electron-phonon coupling matrix elements are given by

$$g^{\text{impurity}}_{i,j}(\boldsymbol{k},\boldsymbol{q}) = \left\langle i,\boldsymbol{k}\left|\frac{4\pi e^2 Z}{\varepsilon(q)(q^2+q^2_{\text{scr}})}\right|j,\boldsymbol{k}+\boldsymbol{q}\right\rangle, \quad (6)$$

where Z is the charge of the ionized dopant and q_{scr} is the screening length. $\varepsilon(q)$ is a model dielectric function[14] given by

$$\varepsilon(q) = 1 + \left[\frac{1}{\varepsilon(0)-1} + d(\frac{q}{q_{\text{TF}}})^2 + \frac{\hbar^2 q^4}{4m^2\omega_p^2}\right]^{-1}. \quad (7)$$

Here d is a parameter taken to be 1.563, q_{TF} the Thomas-Fermi screening length, and ω_p the plasma frequency. The screening length q_{scr} corresponds to Debye screening in the non-degenerate case (concentrations $\leq 10^{18}$ cm^{-3} in SnO_2) and to Thomas-Fermi screening in the degenerate case.

B. Computational details

All calculations were performed with the QUANTUM ESPRESSO code,[15] using norm-conserving pseudopotentials[16] and the local density approximation (LDA)[17] for the exchange-correlation functional. This functional underestimates the band gap, but the shape of the conduction bands, which is important here, is described well. A plane-wave cutoff energy of 90 Ry was used. The phonon frequencies and electron-phonon coupling matrix elements are obtained within density-functional perturbation theory[18] (DFPT) for points on a 20×20×30 grid in the irreducible part of the first Brillouin zone. With this $\boldsymbol{q}$-point grid our results are converged for photon energies starting from 0.62 ev (or equivalently for wavelengths up to 2000 nm). Describing smaller photon energies would require a finer grid. To avoid the computationally expensive double sum over $\mathbf{k}$ and $\boldsymbol{q}$ in Eq.(1), we assume that all free carriers are located at the Γ-point, therefore eliminating the sum over $\mathbf{k}$. The results shown in the figures are all obtained at room temperature (T = 300 K), unless otherwise noted.

We focus here on SnO_2, which has the rutile structure (space group #136, P4/mnm), with 2 formula units per unit cell. The structure can be described with two lattice parameters (a and c), and an internal parameter u which fixes the position of the oxygen atoms. After relaxing the structure we find a to be 4.701 Å, and c to be 3.170 Å. These values are slightly underestimated if

compared to experimental values (a=4.737 Å, c=3.185 Å[19,20]), which is typical for the LDA functional. The band structure along the high-symmetry lines $X-\Gamma$ and $\Gamma-Z$ is shown in Fig. 1(a). Note that in this figure we applied a rigid scissor shift to the conduction bands to match the experimental band gap of SnO_2,[6] since the LDA functional underestimates the band gap. This is only for visual purposes, because we are not studying across-the-gap absorption.

The phonon spectrum calculated using the DFPT method is shown in Fig. 1(b). The phonon frequencies at the zone center are listed in Table I, along with mode symmetries. The phonon frequencies compare very well with previous first-principles results and, more importantly, with experimental measurements, as shown in Table I.

C. Optical transition matrix elements

In order to evaluate the generalized optical matrix elements [Eqs. (2) and (3)], one needs the optical transition elements $\boldsymbol{v_{ij}}$. These can be calculated by using the velocity operator $\boldsymbol{v}^{\rm vel}$, which is defined as

$$\boldsymbol{v}^{\rm vel} = \frac{i}{\hbar}[H, \boldsymbol{r}],$$

and the matrix elements can be calculated by

$$\boldsymbol{v}^{\rm vel}_{ij}(\boldsymbol{k}) = \lim_{q\to 0} \frac{E_j(\boldsymbol{k}+\boldsymbol{q}) - E_i(\boldsymbol{k})}{\hbar q} \times \int \psi^*_{i\boldsymbol{k}}(\boldsymbol{r}) e^{i\boldsymbol{q}\cdot\boldsymbol{r}} \psi_{j,\boldsymbol{k}+\boldsymbol{q}}(\boldsymbol{r}) d\boldsymbol{r}. \quad (8)$$

For the special case of the intraband matrix elements this reduces to

$$\boldsymbol{v}^{\rm vel}_{ii}(\boldsymbol{k}) = \frac{1}{\hbar}\nabla_{\boldsymbol{k}} E_i(\boldsymbol{k}).$$

Using basic quantum mechanics, we can rewrite the expression for $\boldsymbol{v}^{\rm vel}$ as

$$\boldsymbol{v}^{\rm vel} = \boldsymbol{v}^{\rm mom} + \frac{i}{\hbar}[V, \boldsymbol{r}],$$

where V is the external potential, and $\boldsymbol{v}^{\rm mom}$ is the momentum matrix element, defined as

$$\boldsymbol{v}^{\rm mom} = \frac{\boldsymbol{p}}{m} = -\frac{i\hbar}{m}\nabla_{\boldsymbol{r}}.$$

The matrix elements can then be calculated in reciprocal space using

$$\boldsymbol{v}^{\rm mom}_{ij}(\boldsymbol{k}) = \frac{\hbar\boldsymbol{k}}{m}\delta_{ij} + \sum_{\boldsymbol{G}} \frac{\hbar\boldsymbol{G}}{m} c^*_i(\boldsymbol{G}) c_j(\boldsymbol{G}), \quad (9)$$

where c_i are the Fourier coefficients of the wave function,

$$\psi_{n\boldsymbol{k}}(\boldsymbol{r}) = \frac{1}{V}\sum_{\boldsymbol{G}} c_n(\boldsymbol{G}) e^{i(\boldsymbol{k}+\boldsymbol{G})\cdot\boldsymbol{r}}.$$

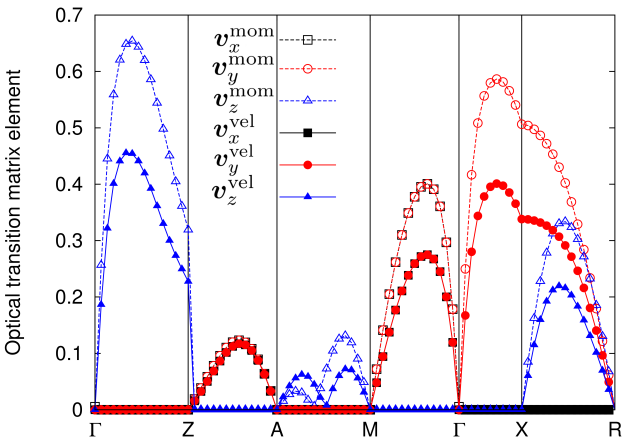

FIG. 2. (Color online) Optical matrix elements for intraband transitions in the conduction band, plotted along high-symmetry lines. The matrix elements are calculated either using momentum ($\boldsymbol{v}^{\rm mom}$) [Eq. (9)] or velocity ($\boldsymbol{v}^{\rm vel}$) [Eq. (8)].

If V commutes with the position operator $\boldsymbol{r}$, either the velocity $\boldsymbol{v}^{\rm vel}$ or the momentum matrix elements $\boldsymbol{v}^{\rm mom}$ can be used to calculate the optical transition matrix elements. However, our first-principles calculations use nonlocal pseudopotentials, and the nonlocal part of the pseudopotential does not commute with the position operator.

Neglecting this commutator leads to a marked difference between the matrix elements obtained with either Eq. (8) or Eq. (9), as illustrated in Fig. 2, where we plot the optical matrix elements for intraband transitions in the conduction band. Degeneracies are taken into account where necessary.

Both matrix elements have the same symmetry, but the values calculated using the momentum operator $\boldsymbol{v}^{\rm mom}$ are distinctly larger than those calculated using the velocity operator $\boldsymbol{v}^{\rm vel}$. Similar observations have been made in the context of the calculation of the dielectric function[28–32] for optical properties.

To avoid having to calculate the $[V, \boldsymbol{r}]$ commutator we always used the velocity matrix elements in this work.

D. Fröhlich model

The task of calculating the absorption coefficient [Eq. (1)] would be greatly simplified if an approximate model for the electron-phonon coupling matrix elements could be used, since a first-principles evaluation of these matrix elements on a finely sampled grid of $\boldsymbol{q}$ points is extremely computationally demanding. The textbook example of such a model is the Fröhlich model for the coupling between longitudinal optical (LO) phonons and electrons. This model describes the interaction between an electron and the electric field generated by an LO

TABLE I. Comparison of calculated phonon frequencies (in cm^{-1}) with other computational and experimental measurements.

Mode	Present calc.	LDA[a]	LDA[b]	GGA[b]	LDA[c]	LDA[d]	Exp.[e]	Exp.[a]	Exp.[f]	Exp.[g]
B_{1g}	102	104	83	90	105	110	121	121	-	119
B_{1u}	147	147	138	134	147	160	-	-	-	-
$E_u^{(1)}$ (TO)	226	223	200	197	242	226	-	-	244	-
$E_u^{(1)}$ (LO)	265	269	252	237	279	-	-	-	276	-
$E_u^{(2)}$ (TO)	279	285	270	253	286	301	-	-	293	-
$E_u^{(2)}$ (LO)	344	335	307	294	406	-	-	-	366	-
A_{2g}	355	360	320	314	366	372	-	-	-	-
A_{2u} (TO)	460	456	457	424	461	510	-	-	477	-
E_g	477	468	462	433	470	500	476	476	476	475
B_{1u}	568	564	553	520	585	501	-	-	-	-
$E_u^{(3)}$ (TO)	600	613	584	538	581	646	-	-	618	-
A_{1g}	638	633	617	578	638	677	637	636	638	636
A_{2u} (LO)	667	670	648	607	657	-	-	-	705	-
$E_u^{(3)}$ (LO)	728	745	712	662	704	-	-	-	770	-
B_{2g}	755	765	734	688	762	785	781	778	782	777

[a] Ref. 21
[b] Ref. 22
[c] Ref. 23
[d] Ref. 24
[e] Ref. 25
[f] Ref. 26
[g] Ref. 27

phonon in a polar material with the expression:[13,33]

$$g_F(\boldsymbol{q}) = \sqrt{\frac{2\pi\hbar\omega_{\rm LO}e^2}{V_{\rm cell}q^2}\left(\frac{1}{\epsilon_\infty}-\frac{1}{\epsilon_0}\right)}, \qquad (10)$$

where $\omega_{\rm LO}$ is the frequency of the LO mode at the Γ point, $V_{\rm cell}$ is the volume of the unit cell, and ϵ_∞ and ϵ_0 are the high-frequency and static dielectric constants. Within this model the electron-phonon coupling matrix element is thus proportional to $1/q$.

Since we have performed calculations of the matrix elements completely from first principles, we are in a position to check the validity and accuracy of the Fröhlich model [Eq. (10)] for describing the electron-phonon coupling. In Fig. 3 we compare the intraband matrix elements (for the lowest conduction band) along two high-symmetry directions, parallel (Γ-Z) and perpendicular (Γ-X) to the c-axis of the rutile structure. SnO_2 has 6 atoms in the unit cell, leading to 18 different phonon modes. For clarity we restrict ourselves to plotting those phonon modes that were found to contribute significantly to the electron-phonon coupling. We labeled these modes according to their character (see Table I for the frequencies of these modes at Γ). We use the experimental dielectric constants (thus taking into account the anisotropy) in the Fröhlich model [Eq. (10)]. Also plotted (red crosses) is the square root of the sum of all first-principles electron-phonon matrix elements. This quantity gives an indication of the total electron-phonon coupling strength, so that we can compare this with the Fröhlich model.

The Fröhlich model [Eq. (10)] and the sum of the modes have a similar $1/q$ behavior, but the Fröhlich model overestimates the electron-phonon coupling matrix elements in the perpendicular direction. It is possible to fit a Fröhlich-like $1/q$ to the sum of modes for both directions, and such a fit clearly shows the anisotropy of the system, as the fitting parameters are different in both directions. Inspection of the contribution of the sep-

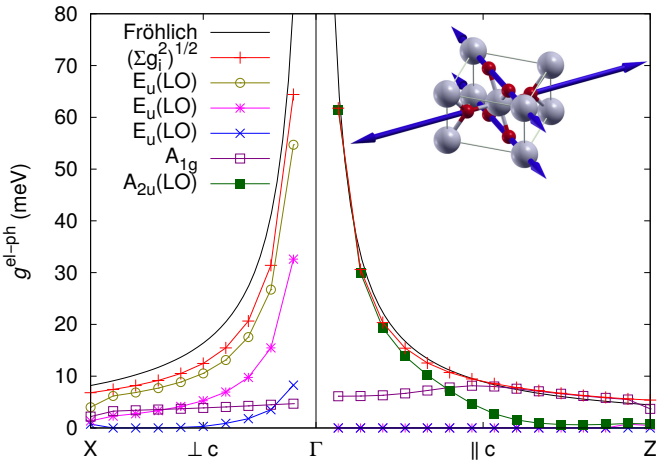

FIG. 3. (Color online) Electron-phonon matrix elements describing coupling between Γ and other points of the first Brillouin zone, plotted along two high-symmetry directions. The Fröhlich model, as described in the text, and the square root of the sum of all first-principles electron-phonon matrix elements are also shown (solid line) The inset shows the displacement pattern of the A_{1g} phonon mode (indicated by arrows). The large (grey) spheres indicate Sn atoms and the smaller (red) spheres O atoms.

arate modes shows that for the perpendicular direction the majority of the electron-phonon coupling is due to the different LO phonon modes (the E_u and A_{2u} modes) and the A_{1g} phonon mode. The latter is a breathing mode, as shown in the inset of Fig. 3. For the parallel direction (Γ-Z) the A_{2u} mode is the only contributing LO phonon mode, and the contribution of the A_{1g} mode becomes dominant for $\boldsymbol{q}$ vectors close to the Brillouin-zone edge (Z). Since the A_{1g} mode is not an LO mode, it is a remarkable coincidence that the sum of all modes gives good agreement with the Fröhlich model for the parallel direction. However, the Fröhlich model [Eq. (10)] was not intended to have a good agreement with the sum of all modes, but rather with the A_{2u} LO mode, and the electron-phonon coupling strength of this mode does not follow the $1/q$ dependence for larger $\boldsymbol{q}$ vectors ($\boldsymbol{q}$ vectors away from the Γ point).

In the following we will use the term Fröhlich model to refer to the use of Eq. (10), as if only a single LO phonon mode contributes. We will also assume that the Fröhlich model can be applied to interband electron-phonon coupling matrix elements.

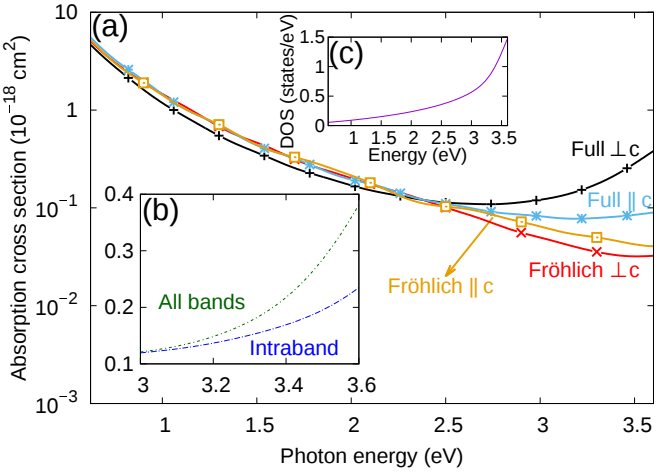

FIG. 4. (Color online) (a) Absorption cross section of SnO_2 obtained using full first-principles calculations of electron-phonon coupling compared with calculations using the Fröhlich model. (b) First-principles absorption cross section for light polarized perpendicular to the c direction, either restricted to the first conduction band (intraband) or taking into account all conduction bands. (c) Density of states for the conduction band.

III. RESULTS

A. Phonon-assisted absorption

In Fig. 4(a) we plot the absorption cross section σ as a function of photon energy; σ is equal to the absorption coefficient α divided by the free-carrier concentration n ($\sigma = \alpha/n$). The electron-phonon interaction is not screened; we will discuss the effect of screening in Sec. III D. Some of these results were previously reported.[11] In the figure we also show the results obtained using the Fröhlich model to describe the electron-phonon interaction in Eqs. (2) and (3). It is clear that use of the Fröhlich model leads to distinct differences in the calculated absorption spectrum. For photon energies below about 2.3 eV, the behavior is similar for the Fröhlich results and the full first-principles results, but significant deviations occur for photon energies larger than 2.3 eV for perpendicularly polarized light and 2.7 eV for parallel-polarized light. In order to understand these deviations we examine the type of transitions needed to have absorption in this region: Fig. 1 shows that this requires transitions from the Γ point to states near the edge of the Brillouin zone. These transitions require phonons with large momentum, and for large q the Fröhlich model seems to yields too small electron-phonon coupling matrix elements, as these are proportional to $1/q$ in the model. While for the two directions shown in Fig. 3 the $1/q$ dependency is accurate, this is not the case for general $\boldsymbol{q}$ vectors with large momentum.

Our first-principles data also show that taking into account only *intraband* transitions, even if including all phonon modes, is not sufficient to describe the increase in absorption, particularly above 3 eV. It is essential to include transitions to the next conduction band, as illustrated in Fig. 4(b). The fact that only the next-higher conduction band needs to be considered in this energy range is evident from the band structure [Fig. 1(a)].

B. Contributions to phonon-assisted absorption

Equation (1) contains two contributions to indirect phonon-assisted absorption: S_1 [Eq. (2)] and S_2 [Eq. (3)]. Additionally, both emission and absorption of a phonon can occur. We now investigate the relative importance of these different processes. To that end we plot the different contributions to the absorption cross section in Fig. 5. Clearly the contribution from phonon emission processes is larger than from phonon absorption processes. This has the important consequence that even at low temperatures there will be absorption of photons by free carriers, as phonon emission can occur at any temperature. Temperature dependence is discussed in detail in Sec. III C. For light polarized perpendicular to c, the S_2 process dominates the absorption cross section at small photon energies, while S_1 dominates at larger energies. For light polarized parallel to c the same trend is observed, but the crossover occurs at higher energies. Note that the total cross section can be smaller than the individual components.

The integral of the delta function in Eq. (1) corresponds to the density of states (DOS) of the conduction band, shifted to slightly lower (higher) energies by the energy of the absorbed (emitted) phonon. The DOS of the conduction band is shown in Fig. 4(c). The DOS increases when the photon energy increases, with a much

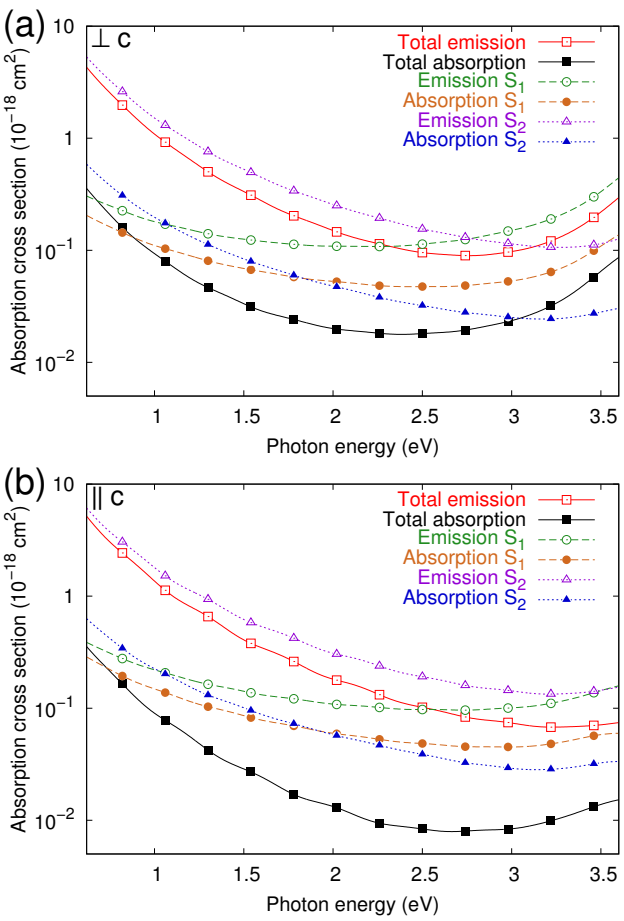

FIG. 5. (Color online) Contributions to the absorption cross section as a function of photon energy, for (a) light polarized perpendicular to the c direction and (b) light polarized parallel to c. Contributions are split according to the components of Eq. (1), S_1 and S_2, as well as according to phonon emission or phonon absorption.

faster increase for energies larger than 3 eV. This rise explains part of the increase in absorption cross section in this energy region for light polarized perpendicular to c. The other part is related to the electron-phonon coupling, which we will discuss shortly. Also the optical coupling matrix elements are important, as exemplified by the parallel component not exhibiting an increase in the absorption cross section, as the transitions from the first conduction band to the second conduction band are dipole forbidden.

The comparison between the Fröhlich model and the full first-principles data in Fig. 4 indicates that for small photon energies (corresponding to long wavelengths) the Fröhlich model provides an adequate description. The physical reason behind this is that the high-frequency LO phonon modes dominate for these photon energies. This can be seen from Fig. 6, where the contribution of several selected phonon modes to the total absorption is shown as a percentage. The oscillatory behavior of some of the curves arises from the difficulty of distinguishing the character of phonon modes that cross other modes or are degenerate at certain points in the Brillouin zone; note the oscillations are not present in the summation curves.

There are distinct differences in the contributing phonon modes for light polarized perpendicular or parallel to the c direction. For perpendicularly polarized light [Fig. 6(a)], the highest LO mode contributes 67% for small photon energies. The contribution of the A_{1g} mode is at most 11% over the range of photon energies. At the same time, phonons with frequencies smaller than 400 cm^{-1} contribute more than 20%, a percentage that increases to 68% for photon energies larger than 3.5 eV. For energies up to 2 eV, the contributions from phonons with frequencies smaller than 400 cm^{-1} consist mostly of LO phonon modes other than the one with the highest frequency (see Table I for the frequencies). This is also illustrated by the curve representing the sum of all LO phonon modes (black circles). For larger photon energies, also other (non-LO) phonon modes start to contribute.

In case of light polarized parallel to c [Fig. 6(b)], the largest contribution to the indirect absorption also originates from the highest LO phonon mode (around 77%) for low photon energies. When the photon energy is increased, the contribution of the A_{1g} mode increases, so that the contribution of the sum of the highest LO mode and this A_{1g} mode contributes more than 60% for photons with an energy of 3.2 eV. This is an important difference compared to perpendicularly polarized light. Another difference is that the contribution of the phonon modes with frequencies smaller than 400 cm^{-1} is small and only becomes larger than 20% for photon energies larger than 2.8 eV.

Given that non-LO phonon modes contribute to the indirect absorption for larger photon energies, it is rather surprising that the Fröhlich model captures these contributions so well (see Fig. 4), only starting to deviate for photon energies larger than 2.3 eV. At this photon energy only 45% (69%) of the total absorption cross section is due to LO phonon modes for the perpendicular (parallel) direction.

C. Temperature dependence

The only term in Eq. (1) that contains a temperature dependence is the factor P [Eq. (5)], which accounts for the carrier and phonon statistics. The phonon occupation number $n_{\nu\boldsymbol{q}}$ is given by

$$n_{\nu\boldsymbol{q}} = \frac{1}{\exp\left(\frac{\hbar\omega_{\boldsymbol{q}}}{k_B T}\right) - 1}, \tag{11}$$

where k_B is the Boltzmann constant and T the temperature. The $\pm$ sign in the first part of Eq. (5), $\left(n_{\nu\boldsymbol{q}} + \frac{1}{2} \pm \frac{1}{2}\right)$, refers to absorption versus emission of

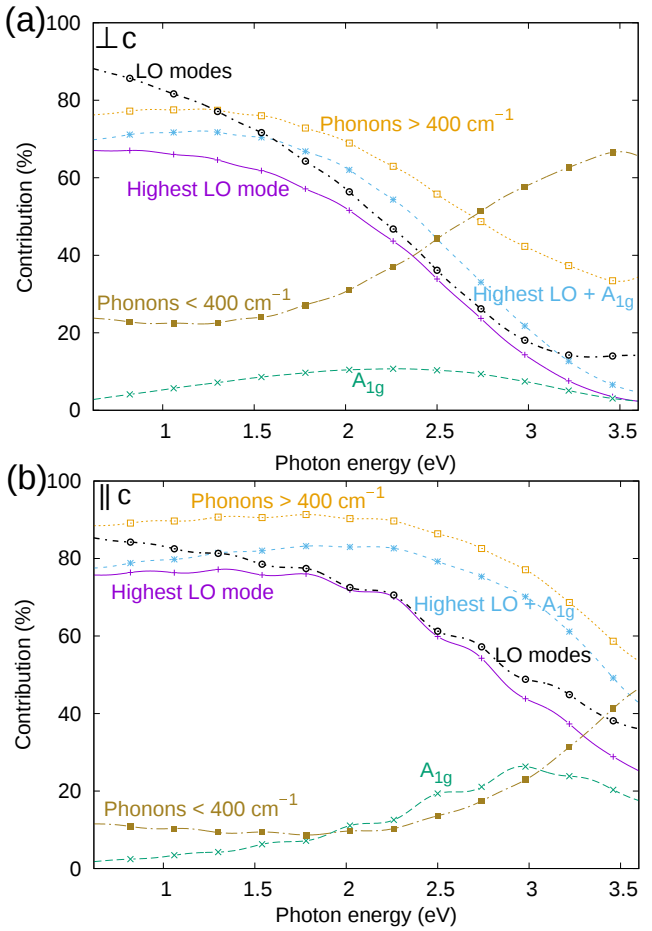

FIG. 6. (Color online) Contribution to the total absorption cross section, in percent, for the highest LO phonon mode, the A_{1g} mode, the sum of the highest LO mode and the A_{1g} mode, the sum of all LO modes, the sum of all phonon modes with frequencies smaller than 400 cm^{-1}, and the sum of all phonon modes with frequencies larger than 400 cm^{-1}, for (a) light polarized perpendicular to the c direction and (b) light polarized parallel to c.

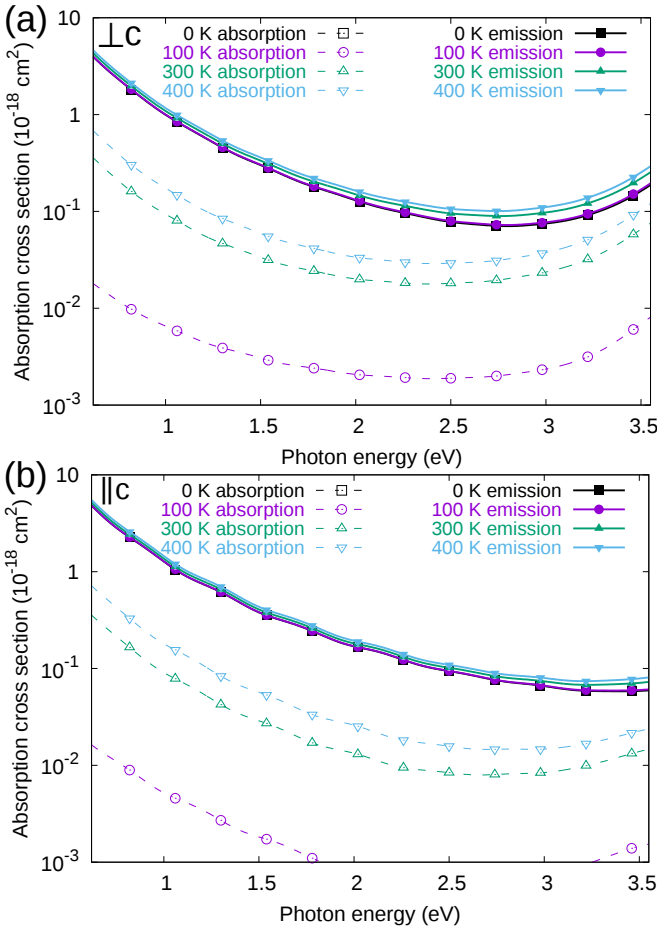

FIG. 7. (Color online) Indirect absorption assisted by the emission (solid lines) or absorption (dashed lines) of phonons, for four different temperatures for (a) light polarized perpendicular to the c direction and (b) light polarized parallel to c.

phonons. The absorption process corresponds to the minus sign, leading to $n_{\nu\boldsymbol{q}}$, while the emission process corresponds to the plus sign, leading to $n_{\nu\boldsymbol{q}}+1$. The difference between these two expressions (the +1) causes the difference in magnitude between the absorption and emission process, as was already evident in Fig. 5.

At 0 K, $n_{\nu\boldsymbol{q}} = 0$, and therefore the contribution to free-carrier absorption assisted by the absorption of phonons is also zero. The emission process is still possible, thanks to the +1 term. When the temperature is increased, $n_{\nu\boldsymbol{q}}$ increases, and both emission and absorption processes increase. This is shown in Fig. 7, where the free-carriers absorption is plotted for four different temperatures, separated into contributions due to absorption (dashed lines) versus emission (solid lines) of phonons. Since the 0 K absorption is zero, it is not visible on the scale used in the figure. Contributions due to emission are always larger than due to absorption, because of the +1 term. Since $n_{\nu\boldsymbol{q}}$ is much smaller than 1 at the temperatures of interest, the temperature dependence for the emission contribution is much weaker than for absorption, explaining why all four curves for emission in Fig. 7 are so close together.

$n_{\nu\boldsymbol{q}}$ depends on the phonon energy, and different phonons contribute to indirect absorption at different photon energies, as discussed in Sec. III B. For small photon energies, mainly the LO phonon modes contribute (see Fig. 6). These LO phonons have the largest energy, so that the dependence of $n_{\nu\boldsymbol{q}}$ on temperature will be smaller, as compared to other phonon modes with lower energies. At higher photon energies, phonon modes with lower energies play a larger role, and hence the temperature dependence will be stronger. These effects can most easily be observed in the emission curves in Fig. 7.

D. Charged-impurity scattering

Free carriers in TCOs can also be scattered by ionized impurities. The presence of such charged centers is unavoidable in TCOs, since donors have to be present to generate the free carriers. Intrinsic defects have also been suggested as dopants, and if they are present, they will scatter free carriers similar to ionized impurities. We describe this charged-impurity scattering process using Eq. (6).

To facilitate the comparison between scattering due to phonons and due to charged impurities, we use the Fröhlich model, as this allows us to also include screening for the phonon-assisted process[13] in a modification of Eq. (10):

$$g_F^{\text{screened}}(\boldsymbol{q}) = \frac{q}{q^2+q_{\text{scr}}^2}\sqrt{\frac{2\pi\hbar\omega_{\text{LO}}e^2}{V_{\text{cell}}}\left(\frac{1}{\epsilon_\infty}-\frac{1}{\epsilon_0}\right)}. \quad (12)$$

From the discussion in Sec. III B we know that the Fröhlich model provides a reliable description up to a photon energy of 2.3 eV.

Figure 8 shows the comparison between indirect absorption due to phonons and due to charged impurities at different concentrations of free carriers. The total absorption cross section will of course contain both contributions. For the purposes of the plot the number of ionized impurities is assumed to be equal to the number of free carriers, i.e., all dopants are fully ionized and contribute one free electron, and no compensating centers are present. Note that if compensating centers are present, they will lower the number of free carriers, while increasing the number of ionized impurities, thereby increasing the relative importance of ionized impurity scattering.

The results for phonon scattering show that screening becomes important for free-carrier concentrations above 10^{18} cm^{-3}. For smaller concentrations the screening length q_{scr} is much smaller than the relevant $\boldsymbol{q}$ vectors, so it does not lead to a considerable decrease in effective matrix elements. Since smaller photon energies also imply smaller $\boldsymbol{q}$ vectors, the effect of screening is much more noticeable for these energies. The screening effects are expected to be similar for our full first-principles results (which deviate from the ones shown in Fig. 8 for energies above 2.3 eV).

The absorption cross section due to charged impurities follows a similar trend as a function of photon energy as the phonon-assisted process. The magnitude of the impurity-induced absorption becomes similar to that of the phonon-assisted absorption at carrier concentrations of 10^{20} cm^{-3}. For impurity concentrations larger than 10^{20} cm^{-3} it becomes the dominant process.

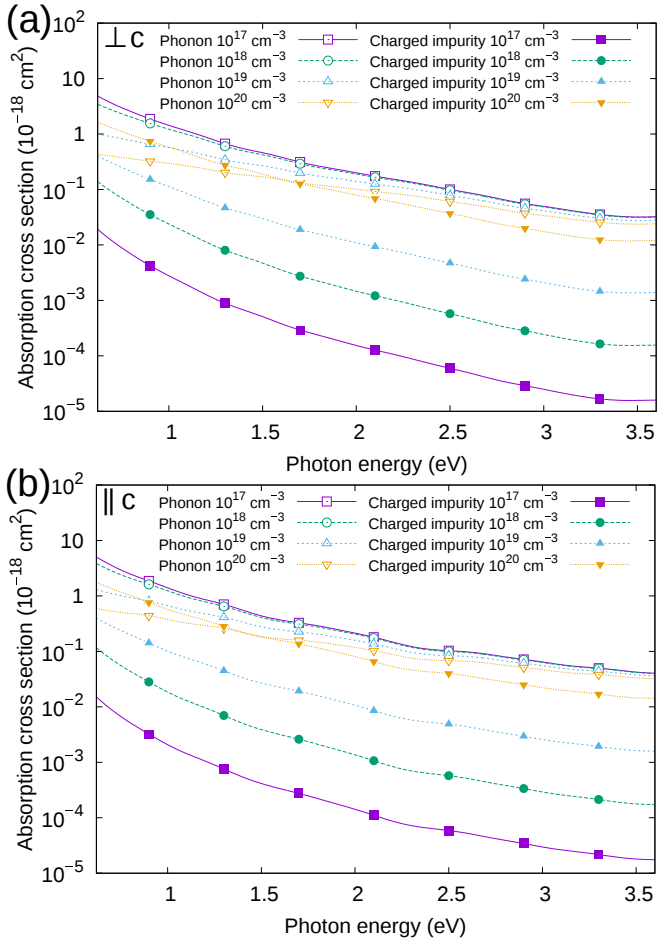

FIG. 8. (Color online) Absorption cross section for different carrier concentrations, for (a) light polarized perpendicular to c, and (b) light polarized parallel to c. Contributions due to electron-phonon scattering (as given by the Fröhlich model, and screened due to the presence of free carriers) (open symbols) and due to charged-impurity scattering (filled symbols) are shown separately.

IV. CONCLUSIONS

We have discussed phonon-assisted and impurity-assisted indirect absorption in transparent conductors, providing first-principles results for SnO_2. We provided a detailed description of the first-principles methodology, emphasizing that velocity matrix elements should be used to calculate the optical transition matrix elements. Because of the nonlocality of the pseudopotentials, using momentum matrix elements without including the commutator of the Hamiltonian with the position operator leads to a significant overestimation of these matrix elements. We investigated which phonon modes play the dominant role in phonon-assisted free-carrier absorption, finding that contributions from the LO phonon modes and the A_{1g} mode are generally most important, except for absorption of light perpendicular to the c direction above 2.3 eV, were low-frequency phonons contribute

most.

We also checked to what extent the Fröhlich model, which only captures LO phonon modes, can approximate the full first-principles results. When applying the model to the indirect phonon-assisted absorption, good agreement with the full first-principles calculation is observed up to photon energies of 2.3 eV; above 2.3 eV, the Fröhlich model underestimates the indirect absorption, as more non-LO phonon modes start to contribute. Processes involving the emission of phonons have the largest contribution to the free-carrier absorption, which implies that phonon-assisted absorption can be significant at low temperatures. The temperature dependence of the free-carrier absorption depends on the phonon energy of the contributing phonons, and therefore also on the photon energy. The dependence is largest for larger photon energies, as lower-frequency phonons contribute more for these photons.

Finally, we also addressed effects of doping. Screening of the electron-phonon interaction becomes important for free-carrier concentrations larger than 10^{18} cm^{-3}. An explicit evaluation shows that the contribution to absorption due to charged-impurity scattering becomes larger than that due to electron-phonon scattering when the impurity concentration exceeds 10^{20} cm^{-3}.

ACKNOWLEDGMENTS

H. P. was supported by the by the Army Research Office (W911NF-13-1-0380). E. K. acknowledges support by the National Science Foundation CAREER award through Grant No. DMR-1254314. Computing resources were provided by the Center for Scientific Computing at the CNSI and MRL: an NSF MRSEC (DMR-1121053) and NSF CNS-0960316, and by the National Energy Research Scientific Computing Center, a DOE Office of Science User Facility supported by the Office of Science of the U.S. Department of Energy under Contract No. DE-AC02-05CH11231.

* peelaers@engineering.ucsb.edu

[1] T. Minami, Semicond. Sci. Technol. **20**, S35 (2005).
[2] M. Batzill and U. Diebold, Prog. Surf. Sci. **79**, 47 (2005).
[3] K. Ellmer, Nat. Photonics **6**, 809 (2012).
[4] E. Fortunato, D. Ginley, H. Hosono, and D. C. Paine, MRS Bull. **32**, 242 (2007).
[5] J. Noffsinger, E. Kioupakis, C. G. Van de Walle, S. G. Louie, and M. L. Cohen, Phys. Rev. Lett. **108**, 167402 (2012).
[6] K. Reimann and M. Steube, Solid State Commun. **105**, 649 (1998).
[7] A. Schleife, J. B. Varley, F. Fuchs, C. Rödl, F. Bechstedt, P. Rinke, A. Janotti, and C. G. Van de Walle, Phys. Rev. B **83**, 035116 (2011).
[8] H. Y. Fan, in *Optical Properties of III-V Compounds. Semiconductors and Semimetals*, Vol. 3, edited by R. K. Willardson and A. C. Beer (Academic Press, New York, 1976) pp. 405–419.
[9] E. Kioupakis, P. Rinke, A. Schleife, F. Bechstedt, and C. G. Van de Walle, Phys. Rev. B **81**, 241201 (2010).
[10] E. Kioupakis, P. Rinke, and C. G. Van de Walle, Appl. Phys. Express **3**, 082101 (2010).
[11] H. Peelaers, E. Kioupakis, and C. G. Van de Walle, Appl. Phys. Lett. **100**, 011914 (2012).
[12] F. Bassani and G. Pastori Parravicini, *Electronic States and Optical Transitions in Solids* (Pergamon Press, 1975).
[13] B. K. Ridley, *Quantum Processes in Semiconductors* (Clarendon Press, Oxford, 1982).
[14] G. Cappellini, R. Del Sole, L. Reining, and F. Bechstedt, Phys. Rev. B **47**, 9892 (1993).
[15] P. Giannozzi, S. Baroni, N. Bonini, M. Calandra, R. Car, C. Cavazzoni, D. Ceresoli, G. L. Chiarotti, M. Cococcioni, I. Dabo, A. D. Corso, S. Fabris, G. Fratesi, S. de Gironcoli, R. Gebauer, U. Gerstmann, C. Gougoussis, A. Kokalj, M. Lazzeri, L. Martin-Samos, N. Marzari, F. Mauri, R. Mazzarello, S. Paolini, A. Pasquarello, L. Paulatto, C. Sbraccia, S. Scandolo, G. Sclauzero, A. P. Seitsonen, A. Smogunov, P. Umari, and R. M. Wentzcovitch, J. Phys.: Condens. Matter **21**, 395502 (2009), http://www.quantum-espresso.org.
[16] N. Troullier and J. L. Martins, Phys. Rev. B **43**, 1993 (1991).
[17] D. M. Ceperley and B. J. Alder, Phys. Rev. Lett. **45**, 566 (1980); J. P. Perdew and A. Zunger, Phys. Rev. B **23**, 5048 (1981).
[18] S. Baroni, S. de Gironcoli, A. Dal Corso, and P. Giannozzi, Rev. Mod. Phys. **73**, 515 (2001).
[19] J. Haines and J. M. Léger, Phys. Rev. B **55**, 11144 (1997).
[20] W. H. Baur, Acta Cryst. **9**, 515 (1956).
[21] T. Lan, C. W. Li, and B. Fultz, Phys. Rev. B **86**, 134302 (2012).
[22] P. D. Borges, L. M. R. Scolfaro, H. W. Leite Alves, E. F. Silva, H. W. L. Alves, and E. F. da Silva, Theor. Chem. Acc. **126**, 39 (2010).
[23] K. Parlinski and Y. Kawazoe, Eur. Phys. J. B **13**, 679 (2000).
[24] R. A. Casali, J. Lasave, M. A. Caravaca, S. Koval, C. A. Ponce, and R. L. Migoni, J. physics. Condens. matter **25**, 135404 (2013).
[25] P. Peercy and B. Morosin, Phys. Rev. B **7**, 2779 (1973).
[26] R. Katiyar, P. Dawson, M. Hargreave, and G. Wilkinson, J. Phys. C **4**, 2421 (1971).
[27] H. Hellwig, A. F. Goncharov, E. Gregoryanz, H. K. Mao, and R. J. Hemley, Phys. Rev. B **67**, 174110 (2003).
[28] M. Rohlfing and S. G. Louie, Phys. Rev. B **62**, 4927 (2000).
[29] B. Adolph, V. I. Gavrilenko, K. Tenelsen, F. Bechstedt, and R. Del Sole, Phys. Rev. B **53**, 9797 (1996).
[30] R. Del Sole and R. Girlanda, Phys. Rev. B **48**, 11789 (1993).
[31] S. Baroni and R. Resta, Phys. Rev. B **33**, 7017 (1986).
[32] M. Hybertsen and S. G. Louie, Phys. Rev. B **35**, 5585 (1987).
[33] O. Madelung, *Introduction to Solid-State Theory* (Springer-Verlag, Berlin, 1978).